Impact of Alkali and Alkali-Earth Cations on Ni-Catalyzed Dimerization of Butene

Andreas Ehrmaier,[a] Laura Löbbert,[a] Maricruz Sanchez-Sanchez,[a] Ricardo Bermejo-Deval,*[a] and Johannes Lercher*[a, b]

The presence of alkali (Na^+ or Li^+) or alkali-earth (Ca^{2+} or Mg^{2+}) cations adjusting the acid-base properties on amorphous silica-alumina influences markedly the catalytic properties of supported Ni for 1-butene dimerization. The low concentration of Brønsted acid sites on these catalysts reduces the double bond isomerization of butene and inhibits the formation of dimethylhexene as primary product. While the alkali and alkali-earth cations act as weak Lewis acid sites, only Ni^{2+} sites are catalytically active for dimerization of 1-butene. *n*-Octene and methylheptene are formed selectively as primary products; dimethylhexene is a secondary product. The open environment of the Ni^{2+} sites does not induce different reaction pathways compared to Ni^{2+} in the pores of zeolites.

Introduction

The conversion of butenes from naphtha steam cracking is of high interest[1] to synthesize branched dimers, for gasoline additives,[1c] or into linear dimers,[2] used as feedstock, e.g. for the production of PVC plasticizers.[1b,3] For the latter purpose, Ni dispersed on amorphous silica-alumina (ASA) is used as a catalyst, obtaining selectivities of approx. 60% to linear and single branched dimers (octene and methylheptene) and 40% to branched dimers (dimethylhexenes).[4]

The ASA support provides both Lewis and Brønsted acid sites, enabling the dispersion and strong interaction of the Ni^{2+} cations. They are the active sites for the dimerization of 1-butene, following a Cossee-Arlman type mechanism.[5] However, isolated Brønsted acid sites (BAS) catalyze the synthesis of branched dimers, via the formation of secondary carbenium ions, as well as by isomerization of 1-butene to 2-butene.[6]

Thus, high selectivity to linear octenes requires the elimination of BAS via ion-exchange for alkali and alkali-earth cations.[7] This step has shown to increase the selectivity in zeolite supported Ni^{2+} catalysts toward linear dimers with C_3 or higher olefins.[5b,8] However, the steric constraints in these catalysts have been hypothesized to selectively stabilize the transition state of linear dimers.[9] Thus, we decided to explore the role of the cations (in their task to reduce Brønsted acidity) in the absence of pore confinement. This study is aimed to differentiate between intrinsic catalytic properties of Ni^{2+} cations in the absence of Brønsted acid sites without constraints of a microporous environment. The impact of alkali and alkali-earth co-cations on a catalyst based on Ni^{2+} cations is explored, therefore, combining detailed acid-base characterization and kinetic measurements.

Results and Discussion

Synthesis and characterization of alkali and alkali earth modified Ni/ASA catalysts

The concentration of Ni^{2+} and the respective co-cations are compiled in Table 1. Amorphous silica-alumina was impregnated with equal concentrations of Ni^{2+} and two different concentrations of Na^+, Ca^{2+}, Li^+, Mg^{2+}. After calcination, NiO particles were observed by XRD (Figure S1, S2). As derived from the width of the XRD peaks, the average diameter of NiO particles increased with increasing co-cation concentration. We

Table 1. Loadings of Ni and the respective co-cations of the catalysts used in this work. (Determined by AAS).

Catalyst	Ni conc. [mmol g^{-1}]	Co-cation conc. [mmol g^{-1}]
Ni/ASA	1.0	
Ni-SiO_2	1.0	
1Na–Ni/ASA	1.0	0.7
1Ca–Ni/ASA	1.0	1.1
1Li–Ni/ASA	1.0	1.4
1Mg–Ni/ASA	1.0	0.8
2Na–Ni/ASA	1.0	2.3
2Ca–Ni/ASA	1.0	2.5
2Li–Ni/ASA	1.0	2.8
2Mg–Ni/ASA	1.0	2.9

[a] A. Ehrmaier, L. Löbbert, M. Sanchez-Sanchez, R. Bermejo-Deval, Dr. J. Lercher
Lehrstuhl für Technische Chemie II
TU München
85748 Garching (Germany)
E-mail: ricardo.bermejo@tum.de
johannes.lercher@ch.tum.de
[b] Dr. J. Lercher
Institute for Integrated Catalysis
Pacific Northwest National Laboratory
P.O. Box 999
Richland, WA 99352 (USA)

Supporting information for this article is available on the WWW under https://doi.org/10.1002/cctc.202000349

© 2020 The Authors. Published by Wiley-VCH Verlag GmbH & Co. KGaA. This is an open access article under the terms of the Creative Commons Attribution License, which permits use, distribution and reproduction in any medium, provided the original work is properly cited.

© 2020 The Authors. Published by Wiley-VCH Verlag GmbH & Co. KGaA

hypothesize that the well-dispersed co-cations interact stronger with ASA and so in turn weaken the interaction between Ni^{2+} and ASA. This is concluded to lead to a higher mobility of Ni^{2+} and, hence, to the formation of larger NiO particles. Also on pure SiO_2 larger NiO particles were observed, highlighting the weak interactions between the Ni^{2+} and silica. Transmission electron microscopy (TEM) showed the formation of NiO particles, ranging from 10–100 nm (Figure S3).

The impregnation solely with Ni^{2+} cations decreased the BET surface area of ASA from 645 to 403 m^2/g (Figure S4, S5), the micropore volume from 0.034 to 0.013 cm^3/g and the mesopore surface area from 689 to 422 m^2/g. A minor relative decrease was observed with respect to the Ni/ASA, with the co-cation concentration (Figure S4A and D), while the pore diameter remained unchanged (Figure S4B). The formation of larger NiO particles in 2Li–Ni/ASA, together with lower BET surface area and smaller mesopores, suggests a high dispersion of the Li cation on the ASA support, blocking its pores.

The IR spectra of adsorbed pyridine were used to evaluate the nature and concentration of acid sites (Figure 1, the 1.25 mmol/g loaded samples are shown in Figure S6). Pyridine adsorption on the parent ASA support (Figure 1B, middle) led to the formation of pyridinium ions with Brønsted acid sites (B–Py) at 1540 and 1637 cm^{-1}.[10] In addition, pyridine hydrogen-bound to weak hydroxyls was observed at 1575 cm^{-1} (H–Py).[10–11] The band at 1621 cm^{-1} is assigned to the 8a vibrational mode of pyridine coordinatively bound to Lewis acid sites (LAS), while the band at 1454 cm^{-1} is attributed to pyridine adsorbed to Al^{3+} LAS (Al-LAS).[10,12]

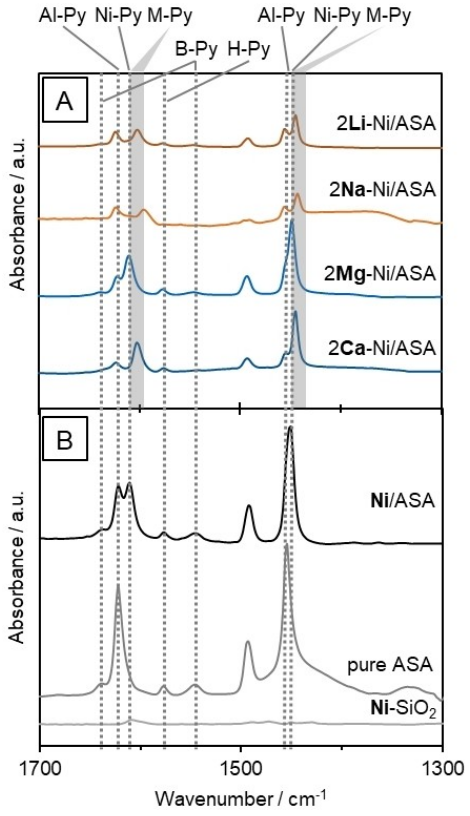

Figure 1. IR spectra of pyridine adsorbed at T = 150 °C on Ni catalysts containing ~2.5 mmol/g of different co-cations (A) and on co-cation free Ni/ASA (B, top) as well as on the pure ASA support (B, middle) or on Ni-SiO_2 (B, bottom). Al–Py: pyridine adsorbed to Al LAS; Ni–Py: pyridine adsorbed to Ni LAS; M–Py: pyridine adsorbed to co-cation LAS, B–Py: pyridine adsorbed to BAS; H–Py: H-bonded pyridine.

The presence of Ni (Figure 1 B, top) hardly changed the total concentration of pyridine bound to LAS and BAS (Figure S7), but significantly influenced the nature of the Lewis acid sites. In addition to the band at 1621 cm^{-1}, a new band was observed at 1610 cm^{-1}, indicative of sites with lower Lewis acid strength.[11a] This band is assigned to pyridine coordinated to a Ni Lewis acid site (Ni–LAS). A small shift was also detected from 1454 to 1450 cm^{-1}. It is hypothesized that this is caused by the increase in concentration of the weaker Ni–LAS. The adsorption of pyridine on NiO/SiO_2 (Figure 1 B, bottom) did not show coordinatively adsorbed pyridine, indicating that pyridine adsorbs less strongly on Ni–LAS. The SiO_2 support does not possess LAS or BAS detectable by adsorbed pyridine.

The co-impregnation of additional cations (Figure 1A) led to minor changes in the IR spectra. The 1621 cm^{-1} band, assigned to the LAS of the ASA support (Al–Py), decreased in intensity. The band at 1610 cm^{-1} (Ni–Py) assigned to the pyridine coordinated to Ni^{2+} cations did not change in intensity. However, an additional third band in that region at lower wavenumbers was observed, assigned to the interaction of pyridine with the co-cations. The highest redshift was observed with the Na^+ (19 cm^{-1}), followed by Ca^{2+}, Li^+ (being both of 10 cm^{-1}) and Mg^{2+} (almost no red-shift). The observed redshift is strongly correlated to the decrease in Sanderson electronegativity of the different co-cations (Figure S8), as following: Mg^{2+} (1.32), Ca^{2+}(0.95), Li^+(0.89) and Na^+(0.84).[13]

In presence of co-cations, the total acid site concentration was significantly lower than on Ni/ASA (Figure 2). The concentration of BAS decreased from 69 μmol/g with Ni/ASA to 0 μmol/g with higher co-cation loading. Increasing concentrations of co-cations decreased the concentration of LAS. The presence of alkali cations (134 and 170 μmol/g with Na^+ and Li^+) had a stronger impact than the presence of alkali earth cations (239 and 346 μmol/g with Ca^{2+} and Mg^{2+}). Using the bands around 1600 cm^{-1} to differentiate between Al–LAS and Ni–LAS (Figure 2, Table S1), it is shown that in presence of Ni^{2+} almost 2/3 of the Lewis acidity was associated with Ni sites. The increase in the concentration of co-cations led to a decrease in the concentration of both Al–LAS and Ni–LAS. This suggests larger NiO particles in the presence of co-cations. A negligible concentration of BAS was observed for all 2.5 mmol/g co-cation loaded samples, suggesting the full exchange of the BAS protons by the alkali and alkali-earth cations.

Dimerization of 1-butene on supported Ni catalysts

The parent ASA was active in the dimerization of 1-butene, forming only methylheptene and dimethylhexene. The catalyst deactivated rapidly (Figure S9). In presence of Ni, the rates increased from 0.12 to 3.17 $mol_{But}\,g^{-1}\,h^{-1}$, (Figure S9 and Figure 3) showing that the Ni^{2+} cations are highly active for

© 2020 The Authors. Published by Wiley-VCH Verlag GmbH & Co. KGaA

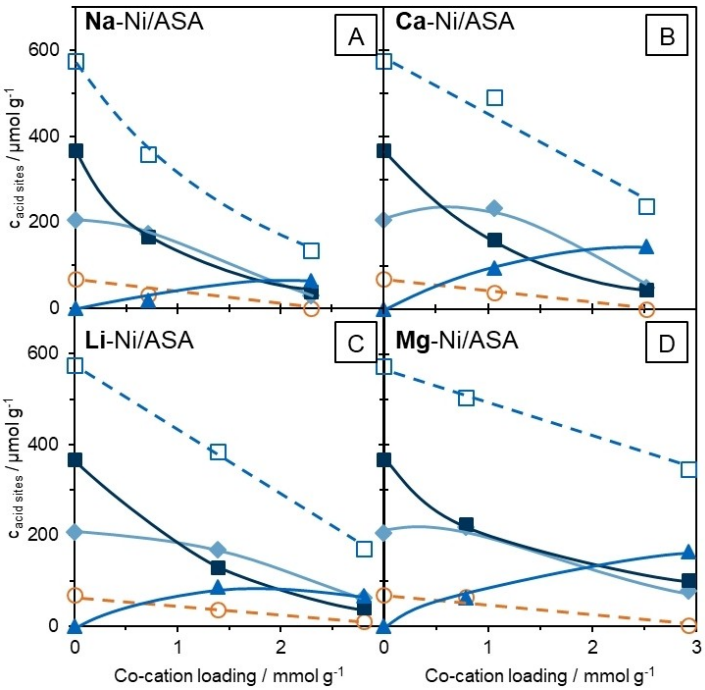

Figure 2. Total concentrations of Lewis (□) and Brønsted (○) acid sites of 6% Ni supported catalysts as a function of different concentrations of co-cations (A: Na–Ni/ASA; B: Ca–Ni/ASA; C: Li–Ni/ASA; D: Mg–Ni/ASA), determined by deconvolution of the peaks at 1450 and 1540 cm^{-1}, respectively. Additionally, the concentration of Lewis acid sites is deconvoluted to Al-Lewis acid sites (Al–Py, ▪, at 1621 cm^{-1}), Ni-Lewis sites (Ni–Py, ▪, at 1610 cm^{-1}) and co-cation based Lewis acid sites (M–Py, ▲, at ~1600 cm^{-1}).

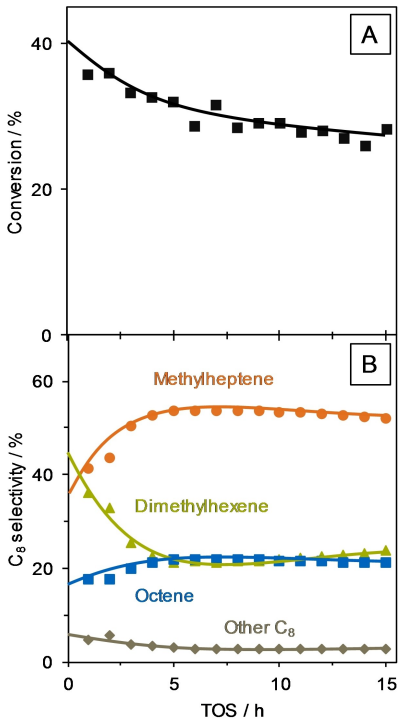

Figure 3. Conversion (A) and dimer selectivity (B) of dimerization of 1-butene over a 6% Ni / ASA supported catalyst (T = 160 °C, p = 50 bar, WHSV = 168 h^{-1}; MHSV = 12 mol_{Butene} mol_{BAS}^{-1} s^{-1}).

dimerization. Surprisingly, Ni–SiO_2 was not active (Figure S10), suggesting that the very large NiO particles are not active in 1-butene dimerization.

Figure 3 shows the conversion of 1-butene (Figure 3A), as well as the selectivity within the dimer fraction (Figure 3B) for Ni/ASA. The catalyst deactivated moderately, decreasing the conversion from 36% to 27% within 15 hours. The selectivity to trimers and tetramers was always below 20% (Figure S11). The selectivity to dimethylhexene (DMH) and methylheptene (MH) was similar within the first hour (41% and 36%, respectively). Over time on stream (TOS), the selectivity to DMH decreased to 23% and the selectivity to MH increased to 52%. The selectivity to n-octene increased slightly from 18 to 21%. The initial higher selectivity to DMH and lower selectivity to MH and n-octene suggests the dimer formation to be catalyzed by both Brønsted and Ni acid sites. The proton catalyzed pathway occurs over a carbenium ion (Scheme S1), and leads to the formation of branched dimers,[6b] as also observed with the parent ASA (Figure S9).[14] The rapid change in selectivity suggests that the BAS sites deactivate fast. To test this hypothesis, the acid site concentration was measured after the reaction (Figure 4) and the BAS concentration was found to have decreased from 69 to 26 µmol/g. The Ni–LAS concentration also decreased from 547 to 422 µmol/g, indicating that both BAS and Ni–LAS were negatively affected by carbon deposits that could be fully removed by calcination. X-ray diffraction analysis of the sample before and after reaction did not indicate significant variation in this process, except for a slight decrease in NiO particle size (Figure S12).

© 2020 The Authors. Published by Wiley-VCH Verlag GmbH & Co. KGaA

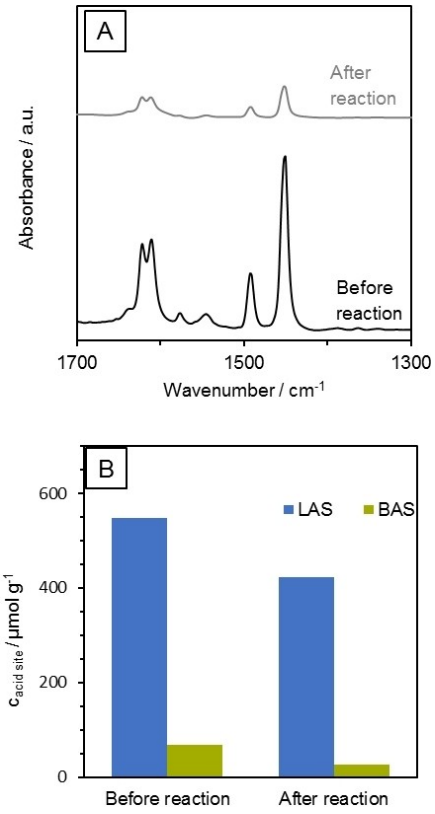

Figure 4. A) IR spectra of adsorbed pyridine (1 mbar at 150 °C) and B) concentration of acid sites of a 6% Ni / ASA catalyst before and after performing the dimerization reaction of 1-butene (T = 160 °C, 50 bar, WHSV = 168 h^{-1}).

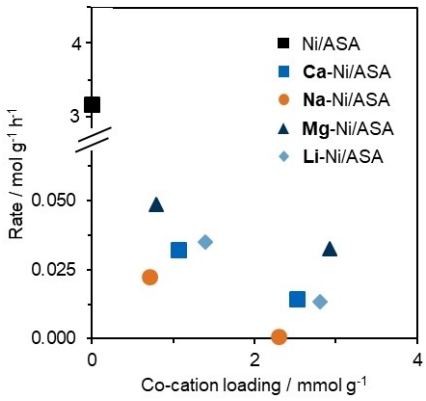

Figure 5. Rate of butene dimerization as function of co-cation loading with 6% Ni on SiO_2-Al_2O_3 (T = 160 °C, p = 50 bar, $WHSV_{co\text{-}cation\ loaded\ catalysts}$ = 6 h^{-1}; $WHSV_{co\text{-}cation\ free\ catalyst}$ = 1389 h^{-1}).

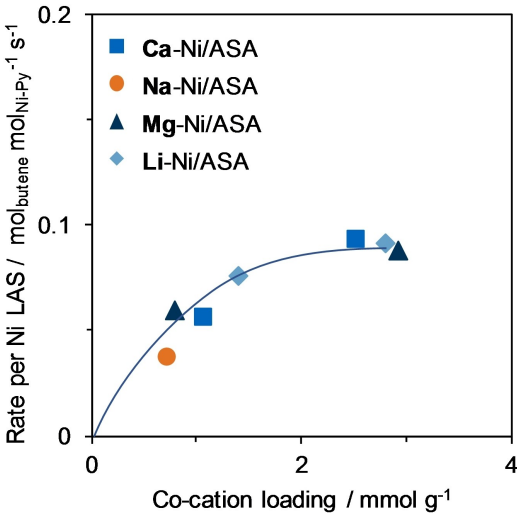

Figure 6. Butene dimerization rate per Ni-Lewis acid sites over different co-cation loaded catalysts with 6% Ni on ASA (T = 160 °C, p = 50 bar, WHSV = 6 h^{-1}).

Impact of co-cations on Ni/ASA on 1-butene dimerization

Figure 5 shows that the dimerization rates decreased in the presence of co-cations, i.e., from 3.17 $mol_{But}\,g^{-1}\,h^{-1}$ with Ni/ASA to ~0.05–0.02 $mol_{But}\,g^{-1}\,h^{-1}$ (Figure S13). While a high deactivation was observed with 2Li–Ni/ASA (70% within 7 hours), the other 2M–Ni/ASA showed only minor deactivation (less than 10% in 7 hours). Hence, a high dispersion of the Ni^{2+} cations on ASA and the absence of Brønsted acid sites is required for high catalyst stability. The reactivity decreased further with higher co-cation loading, independent of the nature of the co-cations. This dependence suggests on first sight that only BAS are active and are gradually eliminated with higher concentration of alkali and alkali-earth cations. On closer inspection one notes, however, that the size of the NiO particles increases with co-cation concentration (Figure S2), leading to a reduction of the concentration of Ni–LAS. This Ni–LAS is hypothesized to be the catalytically active site, with Ni^{2+} cations at exchange positions of the ASA support. Indeed, the rate normalized to the concentration of Ni–LAS (TOF) increased with increasing co-cation concentration (Figure 6) showing that the adjustment of the acid-base properties of the support is beneficial. We speculate that a higher base strength of the support and, hence, a higher electron density at Ni–LAS (weaker Lewis acid strength) is beneficial for the catalytic activity in 1-butene dimerization.

The very low TOF of Na–Ni/ASA is attributed to a very low concentration of Ni–LAS, the reasons for which is currently subject of a separate investigation. Mg^{2+}/ASA (without Ni, Figure S14) did not show catalytic activity for 1-butene dimerization, leading to the conclusion that alkali and alkali earth cations do not catalyze the dimerization of 1-butene under the chosen reaction conditions.

The selectivity to branched products (Figure 7) increased with conversion in a subtly different manner in presence and absence of co-cations. In their absence with Ni/ASA (Figure 7A), initial selectivities show that all three n-octene, methylheptene and dimethylhexene are primary products that change non-linearly with conversion. In the presence of co-cations (~ 2.5 mmol/g, Figure 7B) only n-octene and methylheptene are primary products and dimethylhexene is a secondary product.

© 2020 The Authors. Published by Wiley-VCH Verlag GmbH & Co. KGaA

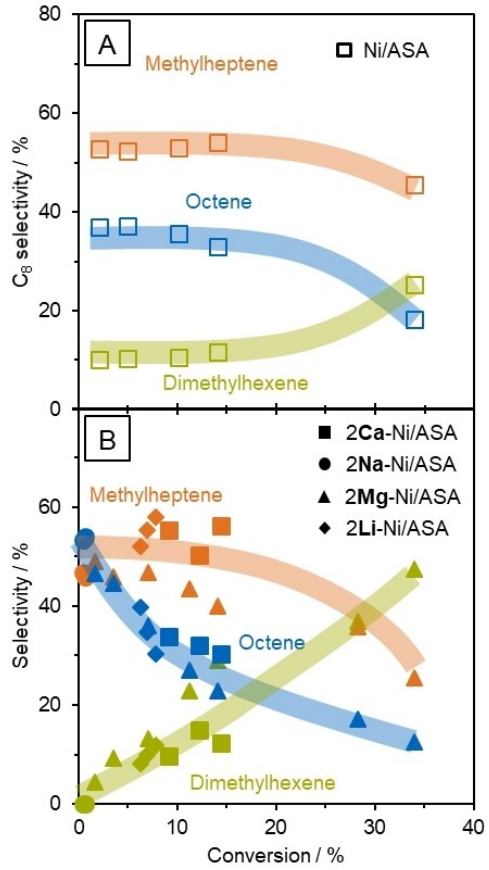

Figure 7. Selectivity of dimers as function of 1-butene conversion over co-cation free Ni (6 wt%) supported catalyst (A) and different co-cation loaded Ni (6 wt%) supported catalysts (B). T = 160 °C, p = 50 bar, $WHSV_A = 1388\ h^{-1}$, $WHSV_B = 6 - 50\ h^{-1}$.

While this indicates that the elimination of BAS also eliminates the direct formation of dimethylhexene, its rapid evolution with conversion on co-cation modified Ni/ASA suggests the presence of an alkali and alkali-earth cation catalyzed isomerization of 1-butene. Considering, for example, the rates of isomerization for 2Mg–Ni/ASA and Ni/ASA (Figure S15), one notes a higher isomerization/dimerization rate ratio in the presence of co-cations, i.e., 0.3 for Ni/ASA and 6.0 for 2Mg–Ni/ASA, respectively. Indeed, Mg on ASA (Mg/ASA) was active in butene isomerization, demonstrating the catalytic activity of the co-cations. In the case of Li–Ni/ASA, despite having NiO particles twice the size of the other catalysts with similar co-cation loading, its catalytic performance does not differ from the other catalysts, suggesting the decrease in BAS concentration is the main driving force changing catalytic activity.

In the absence of steric constraints, the butene dimerization rates and selectivity to linear dimers differ from the microporous environments. The butene dimerization rates for M–Ni/ASA were almost an order of magnitude lower (0.05–0.015 $mol_{But}\,g^{-1}\,h^{-1}$) than in our previous work with M–Ni/LTA (0.13–0.11 $mol_{But}\,g^{-1}\,h^{-1}$). In addition, at 35% conversion selectivities below 10% to dimethylhexene were observed with M–Ni/LTA within the C_8 fraction, while with M–Ni/ASA selectivities to dimethylhexene were around 35–40%. Therefore, we conclude that steric constraints surrounding the active Ni site are able to better stabilize the transition state of butene dimers, especially those leading to the formation of n-octene and methylheptene.

In the absence of BAS we hypothesize that 1-butene is dimerized in a Cossee-Arlman type mechanism with the adsorption of 1-butene on Ni–H and a subsequent insertion and coordination of another butene molecule into the Ni–C bond.[2a,15] Thereby, in the formation of n-octene and methylheptene the initial adsorption would take place as 1,2-insertion into the Ni–H (Scheme 1, left pathway). The subsequent coordination of another 1-butene to the Ni–C bond determines whether n-octene (by 2,1-insertion) or methylheptene (by 1,2-insertion) is formed. The initial 2,1-insertion of 1-butene leads to a branched dimer. Because dimethylhexene is not a primary product in presence of alkali and alkali earth cations, this route can be ruled out.

As isomerization of 1-butene into *cis*- and *trans*-2-butene is occurring, the product 2-butene would adsorb via a 2,3-insertion into the Ni–H, opening this pathway for dimerization (Scheme 1, right pathway, red). This would also lead to the formation of dimethylhexene by subsequent 2,3-insertion. The 2,1-insertion of 1-butene into the Ni–C (formed by 2-butene) results in this case in a secondary pathway for the formation of methylheptene.

Conclusions

The catalytically active sites for 1-butene dimerization have been identified as accessible Ni^{2+} on ASA (Ni–LAS). Ni^{2+} cations in NiO supported on SiO_2 have not been found to have sufficiently high catalytic activity to lead to measurable conversions under the present reaction conditions. The presence of alkali (Na^+ or Li^+) and alkali-earth (Ca^{2+} or Mg^{2+}) co-

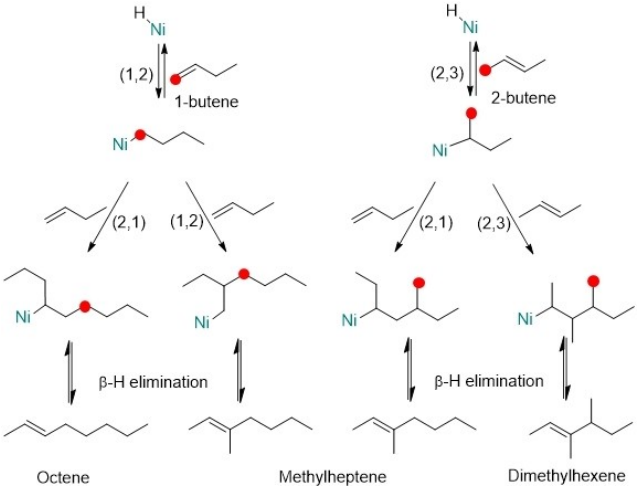

Scheme 1. Reaction pathways for the formation of the different products (octene, methylheptene and dimethylhexene) with 1-butene and 2-butene catalyzed by a Ni–H from Cossee-Arlman site.

© 2020 The Authors. Published by Wiley-VCH Verlag GmbH & Co. KGaA

cations on Ni/ASA blocks BAS that catalyze 1-butene dimerization. This is attributed to an increase in the local base strength. As a negative side effect, the particle size of the supported NiO particles increased, decreasing the concentration of Ni^{2+} cations at exchange positions of the ASA support active in butene dimerization. The alkali- and alkali earth cations increase the initial selectivity to n-octene and methylheptene ($x < 10\,\%$). The co-cations increase, however, also the rate of 1-butene isomerization to 2-butene. In turn, this leads to a rapid increase in the formation rate and selectivity to dimethylhexene. Thus, we conclude that alkali and alkali earth cations are suitable to block BAS catalyzed dimerization of 1-butene, but their ability to induce isomerization of 1-butene does not allow for selective dimerization at higher conversions. Investigations to eliminate this pathway by organic co-reactants (poisons) are under way.

Experimental Section

Catalyst preparation

The catalysts were prepared by incipient wetness impregnation (IWI) of an amorphous ASA support (Sigma-Aldrich, ASA catalyst support, Si/Al = 5.5) material with the aqueous solutions containing all the respective metal salts. The following metal salts were used in the impregnation: $Ni(NO_3)_2$ (Sigma-Aldrich; > 97.0 %), $Mg(NO_3)_2$ (Sigma-Adlrich; > 99.0 %), $Ca(NO_3)_2$ (Merck; > 99.0 %), $LiNO_3$ (Sigma-Adlrich; > 99.0 %), and $NaNO_3$ (Sigma-Adlrich; > 97.0 %). The concentration of the solution was tuned accordingly to the desired metal concentration. The respective co-cation was mixed in the Ni containing impregnation solution, resulting approximately in concentrations of 1 mmol/g Ni and/or ~1.25 mmol/g (nomenclature: 1X–Ni/ASA, X=Na, Li, Ca, Mg) or ~2.5 mmol/g (nomenclature: 2X–Ni/ASA, X=Na, Li, Ca, Mg) of the respective co-cations. After impregnation, the catalyst precursors were dried overnight at 80 °C and subsequently calcined (8 h, rate: 5 °C/min, up to 500 °C in air).

Characterization

Atomic absorption spectroscopic measurements (AAS) were performed in a Solar M5 Dual Flame graphite furnace AAS from ThermoFisher. After drying at 250 °C for 24 h, the samples were dissolved in a mixture of HF and nitric acid and injected in the graphite furnace. A previous calibration was applied to determine the concentration of each of the metals.

X-ray diffraction measurements were performed in a PANalytical Empyreal System diffractometer, equipped with a Cu- Kα radiation source ($K\alpha_1$ line of 1.54 Å; 45 kV and 40 mA)). The diffractograms were measured by the usage of a sample spinner stage in a 2θ range between 5° and 70° (step size: 0.0131303/2θ) at ambient conditions.

The BET specific surface area and pore volume of the zeolite were determined by N_2 sorption. The isotherms were measured at liquid N_2 temperature (77 K) using a PMI automatic sorptometer. The catalyst was activated in vacuum at 473 K for 2 h before measurement. Apparent surface area was calculated by applying the Brunauer-Emmett-Teller (BET) theory with a linear regression between $p/p_0 = 0.01–0.15$. The micro- and mesopores were determined from the t-plot linear regression for t = 5–6 Å.

The adsorption of pyridine was followed by IR in a Nicolet 5700 FT-IR spectrometer, equipped with a liquid N_2 cooled detector. For the measurement, a self-supporting wafer was loaded and activated at 450 °C (rate: 10 °C/min) for 1 h in vacuum. After cooling down to 150 °C, pyridine was equilibrated to 1 mbar for 30 min. Subsequently, the system was evacuated for another 30 min, before measurements. Scans were taken after activation and after outgassing at a resolution of 0.4 cm^{-1} with an average of 250 scans per spectrum. For the calculation of the acid site concentrations, molar extinction coefficients of 0.96 and 0.73 cm/μmol and were used for the characteristic bands of 1450 cm^{-1} (Lewis) and 1540 cm^{-1} (Brønsted),[16] respectively. For the deconvolution of the Lewis acid sites, the bands at 1600 cm^{-1} region were fitted, assuming similar extinction coefficients for all bands of LAS.

Catalytic reactions and kinetics

Catalytic tests were conducted in a fixed bed PFR (id = 3.9 mm), connected to an online GC (Agilent HP 6890, equipped with a 50 m HP-1 column). Prior to GC analysis, H_2 was added to the product stream, which is hydrogenated over a Pt/Al_2O_3 catalyst. A mixture of 15 % i-butane and 85 % 1-butene is introduced by a syringe pump (ISCO model 500 D), temperature is controlled by a Eurotherm 2416 and pressure is controlled using a Tescom back-pressure regulator.

Prior to weighing, the catalyst was dried at 100 °C for 1 h. The catalyst bed was diluted with SiC and fixed in the isothermal zone of the reactor. After activation for 2 h at 450 °C (rate: 10 °C/min) in air, the system was purged with N_2 and pressurized to the desired pressure. Subsequently, the system was flushed with the feed mixture (5 ml/min) for 2 min. After the desired flow rate was set, temperature program and GC measurements were started.

Standard measurement conditions were at 160 °C and 50 bar with a flow rate of butene mixture of 0.04 and catalyst loading of 200 mg to obtain a WHSV of 6 $g\,g^{-1}\,h^{-1}$. The space velocity was varied by changing the catalyst loading and the feed flow rate. The reported rates/conversion/selectivities were obtained after 1 hour on TOS.

i-Butane is inert under reaction conditions applied, and was used as internal standard for normalization of GC areas. Conversion, selectivity and yields are calculated according to the following equations:

$$X = \frac{n(butene)_{in} - n(butene)_{out}}{n(butene)_{in}} \quad (1)$$

$$S = \frac{n(product)_{out}}{n(butene)_{in} - n(butene)_{out}} \; \frac{|\nu_{butene}|}{\nu_{product}} \quad (2)$$

$$Y = \frac{n(product)_{out}}{n(butene)_{in}} \; \frac{|\nu_{butene}|}{\nu_{product}} \quad (3)$$

"Other C_8" refers to unspecified dimethylhexene and methylheptene isomers, different from those shown in Scheme 1.

Acknowledgements

J.A.L was supported by the U.S. Department of Energy (DOE), Office of Science, Office of Basic Energy Sciences (BES), Division of Chemical Sciences, Geosciences and Biosciences (Transdisciplinary Approaches to Realize Novel Catalytic Pathways to Energy Carriers, FWP 47319). RBD would like to acknowledge the Humboldt foundation for the financial support.

© 2020 The Authors. Published by Wiley-VCH Verlag GmbH & Co. KGaA

Conflict of Interest

The authors declare no conflict of interest.

Keywords: Dimerization · Butene Isomerization · Nickel · Silica-Alumina (ASA) · Cossee-Arlman

[1] a) G. C. Bailey, J. A. Reid, Patent US2581228A **1952**; b) A. Behr, Z. Bayrak, S. Peitz, G. Stochniol, D. Maschmeyer, *RSC Adv.* **2015**, *5*, 41372–41376; c) S. Albrecht, D. Kießling, G. Wendt, D. Maschmeyer, F. Nierlich, *Chem. Ing. Tech.* **2005**, *77*, 695–709.
[2] a) E. J. Arlman, *J. Catal.* **1964**, *3*, 89–98; b) P. Beltrame, L. Forni, A. Talamini, G. Zuretti, *Appl. Catal. A* **1994**, *110*, 39–48; c) K. Ziegler, E. Holzkamp, H. Breil, H. Martin, *Angew. Chem.* **1955**, *67*, 541–547.
[3] a) A. Brückner, U. Bentrup, H. Zanthoff, D. Maschmeyer, *J. Catal.* **2009**, *266*, 120–128; b) J. Rabeah, J. Radnik, V. Briois, D. Maschmeyer, G. Stochniol, S. Peitz, H. Reeker, C. La Fontaine, A. Brückner, *ACS Catal.* **2016**, *6*, 8224–8228; c) F. Nadolny, B. Hannebauer, F. Alscher, S. Peitz, W. Reschetilowski, R. Franke, *J. Catal.* **2018**, *367*, 81–94.
[4] S. Raseev, *Thermal and Catalytic Processes in Petroleum Refining*, Marcel Dekker, Inc., New York **2003**.
[5] a) A. Ehrmaier, Y. Liu, S. Peitz, A. Jentys, Y.-H. C. Chin, M. Sanchez-Sanchez, R. Bermejo-Deval, J. Lercher, *ACS Catal.* **2019**, *9*, 315–324; b) A. N. Mlinar, O. C. Ho, G. G. Bong, A. T. Bell, *ChemCatChem* **2013**, *5*, 3139–3147.
[6] a) N. Kumar, P. Mäki-Arvela, T. Yläsalmi, J. Villegas, T. Heikkilä, A. R. Leino, K. Kordás, T. Salmi, D. Yu Murzin, *Microporous Mesoporous Mater.* **2012**, *147*, 127–134; b) M. L. Sarazen, E. Doskocil, E. Iglesia, *J. Catal.* **2016**, *344*, 553–569.
[7] a) H. S. Sherry, H. F. Walton, *J. Phys. Chem.* **1967**, *71*, 1457–1465; b) H. S. Sherry, *Handbook of Zeolite Science and Technology, Marcel Dekker, New York* **2003**, 1007–1061; c) D. Amari, J.-L. Ginoux, L. Bonnetain, *Zeolites* **1994**, *14*, 58–64.
[8] a) A. N. Mlinar, S. Shylesh, O. C. Ho, A. T. Bell, *ACS Catal.* **2013**, *4*, 337–343; b) B. Nkosi, F. T. T. Ng, G. L. Rempel, *Stud. Surf. Sci. Catal., Vol. 97* (Eds.: L. Bonneviot, S. Kaliaguine), Elsevier **1995**, pp. 385–392; c) B. Nkosi, F. T. T. Ng, G. L. Rempel, *Appl. Catal. A* **1997**, *158*, 225–241.
[9] a) A. Ehrmaier, R. Bermejo-Deval, M. Sanchez-Sanchez, Y. Liu, J. A. Lercher, S. Peitz, G. Stochniol, *Vol. EP 3 366 643 A1* (Ed.: EPOrg), EVONIK Degussa GmbH, Technische Universität München **2018**; b) A. Ehrmaier, S. Peitz, M. Sanchez-Sanchez, R. Bermejo de Val, J. Lercher, *Microporous Mesoporous Mater.* **2019**, *284*, 241–246.
[10] G. Ertl, H. Knözinger, F. Schueth, J. Weitkamp, *Handbook of Heterogeneous Catalysis, Vol. 1*, Wiley-VCH Verlag GmbH & Co. KGaA, Weinheim **2008**.
[11] a) C. Morterra, G. Magnacca, *Catal. Today* **1996**, *27*, 497–532; b) H. Knözinger, H. Stolz, *Fortschrittsber. Kolloide Polym.* **1971**, *55*, 16–28; c) H. Stolz, H. Knözinger, *Kolloid Z. Z. Polym.* **1971**, *243*, 71–76.
[12] a) M. Zaki, M. Hasan, F. Al-Sagheer, L. Pasupulety, *In situ FTIR Spectra of Pyridine Adsorbed on SiO2-Al2O3, TiO2, ZrO2 and CeO2: General Considerations for the Identification of Acid Sites on Surfaces of Finely Divided Metal Oxides*, Vol. 190 **2001**; b) C. H. Kline, J. Turkevich, *J. Chem. Phys.* **1944**, *12*, 300–309.
[13] R. T. Sanderson, *J. Chem. Educ.* **1988**, *65*, 112.
[14] M. L. Sarazen, E. Iglesia, *Proc. Natl. Acad. Sci. USA* **2017**, *114*, E3900–E3908.
[15] P. Cossee, *J. Catal.* **1964**, *3*, 80–88.
[16] S. M. Maier, A. Jentys, J. A. Lercher, *J. Phys. Chem. C* **2011**, *115*, 8005–8013.

Manuscript received: February 27, 2020
Revised manuscript received: April 6, 2020
Accepted manuscript online: April 14, 2020
Version of record online: June 3, 2020

© 2020 The Authors. Published by Wiley-VCH Verlag GmbH & Co. KGaA